Investigation of FBG Linear/Angular Acceleration Sensor for Novel Type Inertial Measurement

Byung Kook Kim, Minsu Jang, Jun Sik Kim, Kyumin Kang, Dae-Eun Kim, and Jinseok Kim

***Abstract*—A novel inertial measurement unit (IMU) was proposed to measure the three-axis linear/angular acceleration of a body using six fiber Bragg grating (FBG) optical fiber acceleration sensors sharing the same rotational center. The six acceleration sensors were shown to accurately distinguish between movements in different directions using a vibration generator and rotary motor/encoder device. The results also indicated that the measurement range of the FBG linear acceleration sensor was ±14 g, its average sensitivity was approximately 229.4 pm/g, and its nonlinearity was under 0.05%. Furthermore, the average sensitivity and nonlinearity of the FBG angular acceleration sensor were 21°/s^2/pm and 0.23%, respectively. When measuring linear and angular acceleration, the cross-axis sensitivity of the IMU was within 2.0%. The measurement accuracy of the roll and pitch angle during 360° rotation as well as that of the yaw angle during 720° rotation were both in the range of 0.54%–1.31%. Most of results indicated that the FBG-based IMU sensor was within the performance specifications of an equivalent conventional IMU sensor. Thus, the concept underlying the proposed sensor can be confidently used as a basis to develop a high-precision IMU sensor that is unaffected by electromagnetic interference.**

***Index Terms*—Electromagnetic interference, fiber Bragg grating (FBG) sensor, gyroscope-free, inertial measurement unit (IMU).**

Manuscript received 24 March 2022; revised 27 July 2022; accepted 9 August 2022. Date of publication 24 August 2022; date of current version 23 January 2023. This work was supported in part by the KIST Institutional Program under Grant 2E31642 and Grant 2E3161J, in part by the Korea Medical Device Development Fund grant funded by the Korean Government (The Ministry of Science and ICT, The Ministry of Trade, Industry and Energy, The Ministry of Health and Welfare, and the Ministry of Food and Drug Safety) under Grant KMDF_PR_20200901_0145 and Grant NTIS, KMDF-RnD 1711138281, and in part by the National Research Foundation of Korea grant funded by the Korea government (MSIT) under Grant 2020R1A2C2004714. *(Corresponding authors: Dae-Eun Kim; Jinseok Kim.)*

Byung Kook Kim, Minsu Jang, and Jinseok Kim are with the Center for Bionics, Korea Institute of Science and Technology, Seoul 02792, South Korea (e-mail: cfg10x6p1@kist.re.kr; minsujang@kist.re.kr; jinseok@kist.re.kr).

Jun Sik Kim is with the C&C Process Technical Department, KCTech, Icheon 17332, South Korea (e-mail: twinsdia1@kctech.co.kr).

Kyumin Kang is with the Department of Electrical and Computer Engineering, Sungkyunkwan University (SKKU), Suwon 16419, South Korea (e-mail: zsewqq@g.skku.edu).

Dae-Eun Kim is with the Department of Mechanical Engineering, Yonsei University, Seoul 03722, South Korea (e-mail: kimde@yonsei.ac.kr).

This article has supplementary material provided by the authors and color versions of one or more figures available at https://doi.org/10.1109/TIE.2022.3199918.

Digital Object Identifier 10.1109/TIE.2022.3199918

I. Introduction

THE inertial measurement unit (IMU) sensor is a combination of a three-axis acceleration sensor and an angular velocity sensor. It can be used to indirectly measure the changes in absolute position and rotation angle in three-dimensional (3-D) space by integration of acceleration and angular velocity, respectively [1], [2]. It has been applied to measure the position and rotation angle of target objects in various fields including automotive, drone, aerospace, and motion capture applications [3]. However, conventional IMU sensors manufactured by microelectromechanical systems (MEMS) technology are based on capacitor change detection, which can distort the measured value owing to environmental noise generated by external electromagnetic interference (EMI) and accelerate the drift phenomenon, defined as an accumulated integration error over time [4], [5]. This deterioration of measurement accuracy owing to the drift phenomena induced by EMI severely limits the growth of satellite location tracking systems, future autonomous electric vehicle industries in which large amounts of wireless communication equipment will be installed, and motion capture technology applied indoors [6], [7], [8].

The drift phenomenon is inevitable as long as the measurement obtained by the IMU sensor even has a small error [9]. The causes of the drift phenomenon include numerous factors such as measurement noise, bias, integration method, and accuracy of the angular velocity sensors. To reduce the impact of drift, research has been actively conducted on sensor manufacturing processes and signal processing algorithms [10]. However, previous studies have focused only on reducing the effects of drift phenomena. To fundamentally solve the problem of drift, it is necessary to develop an IMU sensor that departs from the hardware structure of existing MEMS-based IMU sensors to realize a completely new structure and measurement method.

Conventional MEMS-based IMU sensors detect and measure changes in static capacitance according to changes in acceleration or angular velocity [11], [12]. This approach is inevitably influenced by external EMI, adversely affecting the noise property (such as random walk), which is one of the main characteristics of IMU sensors [13]. Though EMI exerts a relatively small influence on the acceleration sensor, when an integration process is performed over time, even very small errors can be accumulated that will eventually have a serious effect on the measured value. Capacitive-type accelerometers and gyroscope sensors will only badly affect random walk, but EMI of conventional IMU sensors fusing with magnetic compasses may cause angular errors of up to 90° or more within a few tens of seconds [14].

Apart from the aforementioned measurement noise caused by EMI, MEMS-based IMU sensors are known to exhibit large errors owing to the use of relatively inaccurate gyroscope sensors [15]. A gyroscope sensor simply measures the physical quantity of angular speed without a reference value, potentially introducing greater errors in roll, pitch angle measurements than an acceleration sensor, which measures gravitational acceleration as its reference value to determine the change in the roll and pitch angles (orientation) of an object [16]. For this reason, some researchers expect that IMU sensors without gyroscopes will be increasingly used in future industries [17]. Furthermore, some researchers have argued that in certain high angular acceleration environments, estimations based on angular acceleration data obtained from only acceleration sensors is more advantageous than measurements collected by conventional MEMS gyroscopes [18]. Although technology to increase the accuracy of IMU sensors through high-precision fiber optic gyroscope sensors using the Sagnac effect has been commercialized to realize more accurate angular tracking of objects, its application in cost-effective industry is limited owing to its extremely high cost and the limited prospect for the small size device [19].

Therefore, a novel three-axis IMU sensor composed of six fiber Bragg grating (FBG) optical linear/angular acceleration sensors unaffected by EMI and gyroscope-free sensor was evaluated in this study. The experimental and analytical results obtained for the proposed FBG-based system were accordingly examined to determine the possibility of its use as an IMU sensor.

II. Sensor Design and Fabrication

A. Sensor Concept Design

Fig. 1 shows the conceptual design of the proposed FBG linear/angular acceleration sensor. Two cantilever-type FBG acceleration sensors are placed in each axial direction. These sensors are deformed when an external acceleration is applied to the mass, and the magnitude of the acceleration is determined by measuring the strain of the cantilever beam using the FBG sensor. The accelerations measured using this method can be divided into two types: linear acceleration and angular acceleration. A single direction of linear movement (x, y, and z) or angular movement (roll, pitch, and yaw) will always deform only the two cantilevers corresponding to that movement. Therefore, in the case of a single direction acceleration, the amount of acceleration can be determined using the average value of the data obtained for two cantilever beams. Even if multiple complex movements occur simultaneously, at least one cantilever will consistently serve as an independent sensor, allowing the direction of movement to be distinguished. Once the direction of movement is determined by the concept of the FBG linear/angular acceleration sensor, as shown in Fig. 1, the magnitude of the movement can be determined by following the conventional method, in which the linear/angular acceleration values obtained from the deformed cantilever are filtered and twice integrated to estimate changes in the position and rotation angle of the object.

Roll and pitch angle measurements can of course be estimated directly using the angular acceleration, but it is more effective to measure them against gravitational acceleration [20]. The FBG acceleration sensor is able to measure gravity, and when rotation occurs in the roll and pitch directions, the measurement value of gravity changes. Therefore, the change in roll and pitch angles can also be measured by an acceleration sensor that measures gravity. Using this linear/angular acceleration measurement mechanism, inertial measurements can be performed.

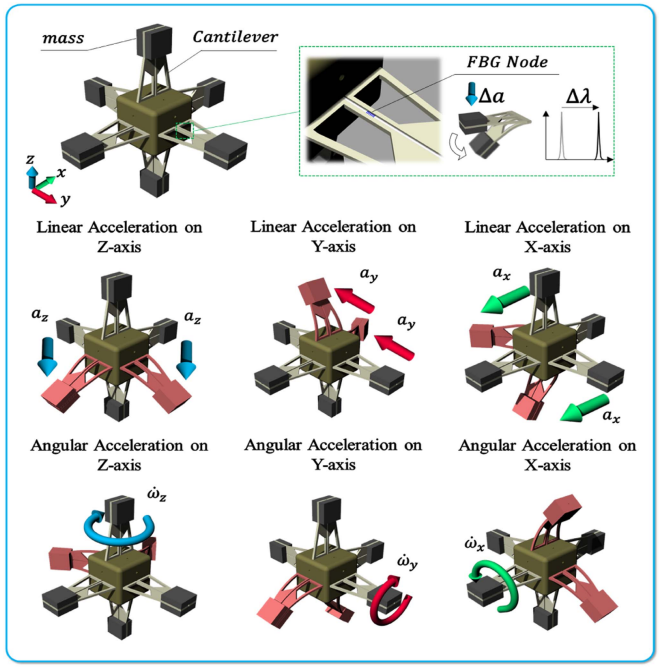

Fig. 1. Structural concept of the proposed FBG linear/angular acceleration sensor and its three-axis sensing mechanism.

B. Analytical Model

A simple 3-D mass–cantilever model was employed to conduct an analytical investigation of the proposed sensor. A mass–cantilever system refers to a system that is fixed on one end and has a free end with an attached mass on the other end. To establish a more accurate analytical model, a system in which FBG fiber optic sensors are embedded inside the cantilever beam was considered. The wavelength change of the FBG optical fiber sensor can be defined by the following expression [21]:

$$\frac{\Delta\lambda_B}{\lambda_B} = (1 - p_e)\ \varepsilon_a + (\alpha + \xi)\,\Delta T \tag{1}$$

where $\Delta\lambda_B$ is the wavelength change of the FBG sensor and λ_B is the center wavelength of the FBG sensors used for experiments. Equation (1) shows that the wavelength change of the FBG sensor is affected by the axial strain (ε_a) and temperature change (ΔT), and the factors affecting the slope of the wavelength change rate are the photoelastic constant (p_e) and the summation of the thermal expansion coefficient (α) and thermo-optic coefficient (ξ).

All experiments evaluating linear/angular acceleration were conducted under constant room temperature conditions, and the sensors were protected from being directly exposed to the

outside by a cap; therefore, the wavelength change rate owing to temperature change was not considered in this study. For more information on the temperature effects, it is described in detail in Fig. S1 in the Supplementary material. The relationship between the axial strain and vertical deflection when the acceleration is applied to the cantilever beam can therefore be expressed as follows:

$$\varepsilon_a = \frac{tM(x)}{2EI_2}, \tag{2}$$

$$M(x) = \frac{3}{L^3}(L-x)EI_2 y, \tag{3}$$

$$\varepsilon_a = \frac{3t}{2L^3}(L-d)y \tag{4}$$

where $M(x)$ is the moment at a specific point located a fixed distance along the cantilever, t is the thickness of the cantilever, E and I_2 are the elastic modulus of the cantilever material and cross-sectional secondary moment, respectively, L is the length of the cantilever, d is the distance from the fixed end of the cantilever to the FBG node, and y is the vertical deflection of the mass owing to the deformation of the cantilever.

Through the relational expressions developed thus far, the wavelength change measured by the FBG sensor according to the vertical deflection at the free end of the cantilever beam can be expressed as follows:

$$\Delta\lambda_B = \frac{3\lambda_B(1-p_e)(t)(L-d)}{2L^3}\eta_1\eta_2 y. \tag{5}$$

Equation (5) was obtained from the combination of (1) and (4), with the addition of the terms η_1 and η_2, where η_1 is the ratio of the actual strain in the FBG sensor embedded in the cantilever to the measured strain, calculated based on related literature [22], and η_2 represents the strain reduction ratio according to the distance from the FBG sensor to the neutral axis of the cantilever cross section. If the FBG sensor is integrally embedded with the cantilever beam, it will experience a reduction in strain according to the offset distance from the neutral axis of the cross section—η_2 defines this reduction as a coefficient.

To develop the FBG wavelength change in relation to the applied acceleration rather than the vertical deflection owing to the deformation of the cantilever beam, the relationship between the force acting on a specific point along the cantilever beam and the vertical deflection of the cantilever beam is employed as follows:

$$P = ma = \frac{6EI_2}{l_a^2(3L-l_a)}y \tag{6}$$

where $l_a$is distance from the fixed end to the point where the force P applied. The linear acceleration applied to the cantilever can be expressed according to its relationship with the vertical deflection of the cantilever using (6). And by combining (5) and (6), the wavelength change according to the acceleration can be obtained as follows:

$$a = \frac{6EI_2}{ml_a^2(3L-l_a)}\frac{2L^3}{3\lambda_B(1-p_e)(t)(L-d)\eta_1\eta_2}\Delta\lambda_B. \tag{7}$$

When the cantilever which has the mass rotates around a particular point, inertia causes tangential acceleration from the center of mass. Thus, the cantilever will be deformed by the generated tangential acceleration, and wavelength changes by the angular acceleration will occur. Finally, governing expressions related to this phenomenon are developed through the following equation:

$$a = r\dot{\omega}, \tag{8}$$

$$\dot{\omega} = \frac{6EI_2}{mrl_a^2(3L-l_a)}\frac{2L^3}{3\lambda_B(1-p_e)(t)(L-d)\eta_1\eta_2}\Delta\lambda_B. \tag{9}$$

Here, $\dot{\omega}$ is the angular acceleration generated at the center of rotation and r is the distance from the center of rotation to the center of mass. Note the difference between L and l_a and r. L is the length of the cantilever and l_a is the distance from the end tip of the cantilever to the center of the mass. In this study, it has a relationship of $L = l_a + 2.5$ mm and $r = L + 2.32$ mm.

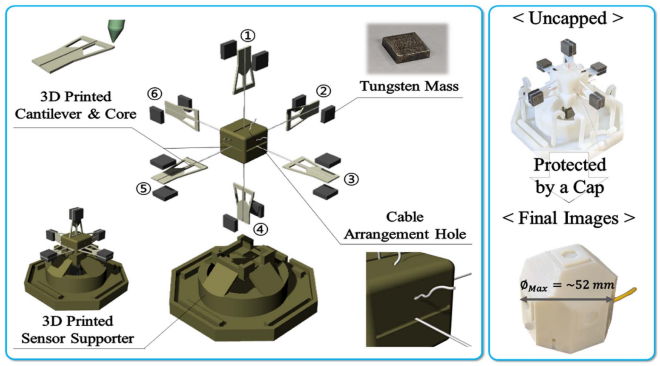

Fig. 2. (a) Assembly diagrams of six FBG acceleration sensors and functions of each assembly process. (b) Manufactured FBG linear/angular acceleration sensors and protected version.

C. Fabrication Procedure

The manufacturing procedure shown in Fig. 2 was employed to produce the proposed FBG-based linear/angular acceleration sensor. As shown in Fig. 2(a), cantilevers were manufactured from a 3-D model using a 3-D printer with a maximum resolution of approximately 16 μm. VeroWhitePlus (RGD835) and SUP705 were used as a build material and support material, respectively, for the 3-D printer based on PolyJet technology. The manufactured cantilevers were output from the single material and the high-quality mode.

Each manufactured cantilever was engraved with a square groove into which an FBG sensor would be inserted. The sensor was attached to the cantilever by compressing both sides of the cantilever together with a glass slide, then filling the remaining space between the groove and FBG sensor with a liquid epoxy and cured using ultraviolet light. This method realized the integration of the FBG sensor and cantilever into an FBG acceleration sensor, and a mass–cantilever-type FBG acceleration sensor was then manufactured by adding a 5.0 $\times$ 5.0 $\times$ 5.0 mm^3 tungsten mass (99% purity) to the free end of the cantilever. When the number of the cantilever is assigned

as shown in Fig. 2(a), the weights of the mass attached to each cantilever were measured to be 1 : 1.465, 2 : 1.500, 3 : 1.510, 4 : 1.508, 5 : 1.480, and 6 : 1.479 g using micro balance. As each manufactured FBG acceleration sensor can detect changes in acceleration in a single-axis direction, six sensors were employed to measure three-axis linear/angular acceleration. The final assembled sensor is shown with and without its protective cap in Fig. 2(b). The maximum length, width, and height of the manufactured FBG linear/angular acceleration sensor were the same at ∼51.71 mm. The cap of the manufactured sensor was fabricated using a 3-D printer with hexagonal sockets engraved in the six directions identical to the axial directions of the six cantilever beams, and linear/angular acceleration experiments were conducted using the sockets to affix the testing equipment. All experiments were conducted at room temperature (21°C) and relative humidity (30%).

III. Experiments and Results

A. Experimental Setup

The sensor module, interrogator, and signal processing algorithms were prepared for the experiments. The central wavelengths of the six FBG sensors used in the proposed linear/angular acceleration sensor were all within the C-band (1530–1565 nm) range. The single-mode optical fibers for the six FBG sensors had central wavelengths of 1532, 1535.8, 1539.6, 1543.4, 1547.2, and 1551 nm with a total diameter of ∼250 μm and a node length of 3 mm. The commercial four-channel interrogator was used to measure the wavelength change of the FBG sensors. The measurement range of the commercial interrogators was approximately 40 nm (1528–1568 nm), with a sampling frequency of 1.25 kHz and wavelength measurement stability within ∼5 pm. The data of the linear acceleration and the angular acceleration experiment were postprocessed through a relatively high sampling frequency (1.25 kHz) provided by the software of interrogator, but when measuring roll/pitch angle, A real-time data processing algorithm was needed. Therefore, the roll/pitch angle were calculated through C++ program that processes and analyzes data in real time. C++ based program obtained the summation of 15 or 20 random data packets through the interrogator software via UDP communication, and the actual value used in the experiments were obtained by dividing the packet value by the number of packets, which leads the sampling frequency of about 70 Hz and average filtering effect.

The most basic experiment performed to evaluate the FBG linear/angular acceleration sensor was the linear acceleration evaluation. Indeed, because the measurement of angular acceleration also relies upon the linear acceleration in the direction tangential to the rotation, the linear acceleration must be fully evaluated first. Fig. 3(a) and (b) shows the vibration test configuration used to evaluate the cross-axis sensitivity, linearity, and sensor sensitivity of the linear acceleration measurement obtained using the manufactured FBG linear/angular acceleration sensor through an acceleration analysis of sinusoidal waveforms over time. A vibration generator was used to generate vibration

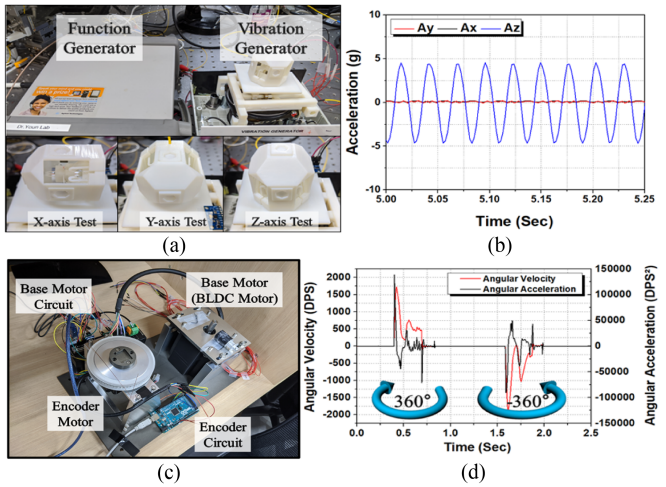

Fig. 3. Linear and angular acceleration sensor tester configuration. (a) Vibration tester for linear acceleration evaluation. (b) Tilt corrected vibration acceleration data measured using MEMS IMU sensor. (c) BLDC, encoder motor for angular acceleration evaluation. (d) Gyroscope data when rotated 360 degrees each in CW/CCW direction (where, DPS is degree per seconds.).

displacement in a sinusoidal shape up/down relative to the direction of gravity. The FBG linear/angular acceleration experiments were conducted in the three linear measurement directions, as shown in Fig. 3(a). When an MEMS-based IMU sensor (automotive grade) was used as a reference, the maximum tilt effect generated by the vibration generator was about 6.15%; after minimizing the tilt using 3-D printed jigs and bearings, the maximum tilt effect was reduced to 2.80%. Because the MEMS-based IMU sensor had a maximum cross-axis sensitivity of ±2.00%, it was confirmed that the effect of the vibration generator tilt itself was a maximum of 0.80% after correction. This corrected result is shown in Fig. 3(b).

Fig. 3(c) and (d) show the configuration of the test equipment used to perform the angular acceleration evaluation of the sensor using a brushless direct current (BLDC) motor. To minimize the influence of external vibrations and tilting of the device, the angular acceleration tester was divided into two motor parts: the base motor and the encoder motor. The base motor used for rotation was a BLDC motor of the BLVM620 series of up to 200 W, and the encoder motor was a BL4241E1K motor with a sensitivity of 1000 channel per rotation through the hall sensor type encoder. When rotation occurs in the base motor (BLDC motor), the rotational force is transferred to the encoder motor through a pulley. Thus, when the encoder motor rotates according to the rotational force, a change in the rotation angle is obtained with respect to the time axis. Changes in the encoder angles over time can be converted into angular velocity and angular acceleration through differentiation over the time, and then compared with the angular acceleration values obtained by the FBG linear/angular acceleration sensors. In this study, angular velocity and acceleration was evaluated through 360° clockwise (CW) and counterclockwise (CCW) rotations as shown in Fig. 3(d).

B. Resonant Frequency Analysis

The resonant frequency of the sensor is a very important factor that can determine the operating area in vibration measurement. In addition, the resonant frequency, mainly as an angular acceleration measurement, is a very important characteristic that can be used to remove the vibration component of the cantilever beam generated during rotation. The determined resonant frequency is used as a constant parameter for the notch filter and can remove resonant vibration component generated from not only angular acceleration but also other movements. Accordingly, noise generated by the vibration component during the integration process may also be reduced, and thus, it must be discussed. An experimental method and an analytical method were introduced to obtain the resonant frequency of the FBG linear acceleration/angle acceleration sensor. After generating free vibration on six cantilevers by applying an impact to the FBG linear/angular acceleration sensor, the first-order resonant frequency was calculated to be about 47.7 $\pm$ 1.6 Hz by calculating the vibration period. Since the resonant frequency is dominantly determined by the shape and mass of the cantilevers, the resonant frequency of the next order was also calculated through the analytical method after confirming the similarity (46.4 Hz) of the first-order resonant frequencies between the experimental and analytical methods. Since only the first-order resonant frequency is required for the application of the notch filter used in this study, the resonant frequency obtained through the analytical method was adopted as a parameter for notch filter, and the detailed results and data of this process are shown in Fig. S2 of the Supplementary material.

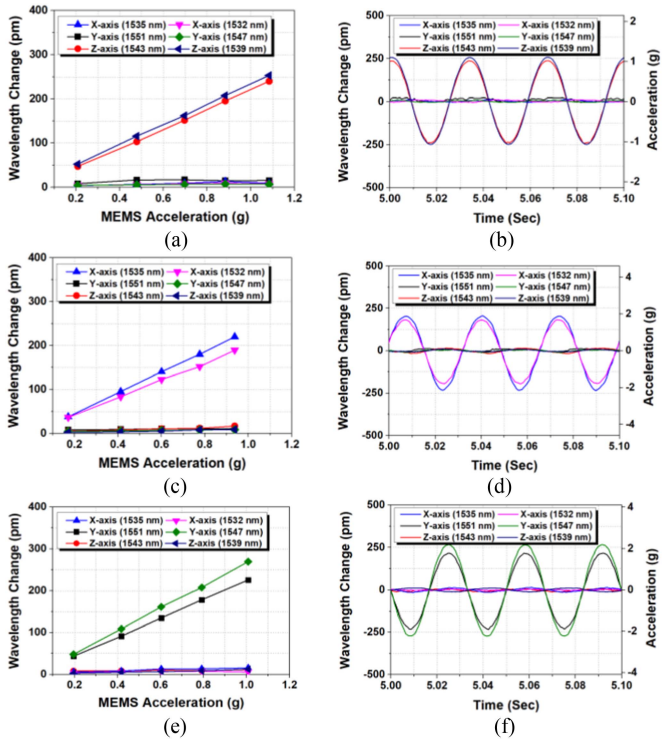

Fig. 4. (a) Wavelength changes induced according to vibration displacement along the *z*-axis and (b) corresponding wavelength shift with acceleration change over time. (c) Wavelength induced according to vibration displacement along the *x*-axis and (d) corresponding wavelength shift with acceleration change over time. (e) Wavelength induced according to vibration displacement along the *z*-axis and (f) corresponding wavelength shift with acceleration change over time.

C. Evaluation As an Acceleration Sensor

The linear acceleration measurement of the FBG linear/angular acceleration sensor were evaluated as shown in Fig. 4 by applying vibration displacements in the *x*-, *y*-, and *z*-axis directions using the linear acceleration test device described in Fig. 3(a). Fig. 4(a), (c), and (e) depict the wavelength changes measured by the FBG linear/angular acceleration sensors according to the changes in acceleration values measured by the MEMS IMU sensors. When acceleration occurs in the *z*-axis direction, the wavelength change of the corresponding two cantilevers (1543 and 1539 nm) was the largest, and the largest wavelength change in the *x*-axis direction was 1535 and 1532 nm, and the *y*-axis was 1547 and 1551 nm. These results confirm the accuracy of the initial design concept, which assumed that when an acceleration acts in a single direction, only the two cantilevers corresponding to that same direction will be deformed. The wavelength change measured by the FBG acceleration sensor according to the applied acceleration change can be defined as the sensor sensitivity as follows:

$$S_{x,\,y,\,z} = \frac{\Delta\lambda_B}{\Delta a} \tag{10}$$

where $S_{x,\,y,\,z}$ represents the sensor sensitivity according to the linear acceleration along the *x*-, *y*-, or *z*-axes. Through (10), it can be seen that the sensor sensitivity is the wavelength change of the FBG sensor according to the change of applied acceleration. For example, if the wavelength changes of 200 pm occurs when an applied acceleration of 1 g (approximately 9.81 m/s) is changed, this FBG acceleration sensor has a sensitivity of 200 pm/g. The sensor sensitivity measured in this method is used to replace the wavelength change obtained through the FBG interrogator to the acceleration change. Moreover, the reliability of the sensor can be verified through the linearity of the wavelength change according to the change in acceleration, and it was calculated by confirming how linearly the wavelength changed according to the acceleration changed.

Using (10) and Fig. 4(a), (c), and (e), the sensor sensitivity for *z*-axis directions (1543 and 1539 nm cantilevers) was 220.6 and 239.0 pm/g, with linearity of 99.97 and 99.96%. For *x*-axis (1535 and 1532 nm), sensitivity was 230.1 and 230.2 pm/g with linearity of 99.99 and 99.85%. For *z*-axis (1547 and 1551 nm), the sensitivity was 260.7 and 222.7 pm/g with the linearity of 99.96 and 98.00%, respectively. Looking at the measured values, in addition to the two acceleration sensors corresponding to the primary direction of movement, slight wavelength changes were generated in the other sensors (nonprimary directions); this is called cross-axis sensitivity.

The influence of cross-axis sensitivity is clearly illustrated in Fig. 4(b), (d), and (f). These graphs show that under an applied

acceleration, significant wavelength changes were generated over time in the two sensors corresponding to the primary direction of motion, while the other four sensors exhibited only slight changes in their wavelengths because they were not governed by the motion in the primary direction. When vibration was applied in the z-axis direction, the cross-axis sensitivities of the sensors corresponding to the x-and y-axes were 3.5% and 4.5%, respectively. For x-axis direction, the cross-axis sensitivities corresponding to the z- and y-axes were 6.3% and 4.8%, respectively. For y-axis direction, the cross-axis sensitivities of the x- and z-axes were 4.3% and 4.8%, respectively. The overall average cross-axis sensitivity of the FBG linear/angular acceleration was thus determined to be 4.7%. According to article [23], the maximum allowable range of cross-axis sensitivity is approximately 5.0%; in the case of MEMS-based IMU sensors, the cross-axis sensitivity has typically been maintained at ±2.0%. The FBG linear/angular acceleration sensor therefore exhibited relatively high levels of cross-axis sensitivity, but this could be sufficiently compensated for using signal processing [24].

The cross-axis sensitivity can be defined as the ratio of the magnitude of the acceleration sensor signals in the nonprimary directions to the magnitude of the acceleration sensor signals in the primary direction. Based on this definition, a generalized relationship compensating for the cross-axis sensitivity can be established for the x-axis as follows:

$$\lambda_{C\_N} = \lambda_{X\_N} \pm \Delta S_{C\_YN} \frac{\Delta\lambda_Y}{\Delta\lambda_{X+Y+Z}} \pm \Delta S_{C\_ZN} \frac{\Delta\lambda_Z}{\Delta\lambda_{X+Y+Z}} \tag{11}$$

where λ_{C_N} is the wavelength value of the specific node in primary vibration direction where the cross-axis sensitivity is being compensated for, λ_{X_N} is the measured wavelength value of a different node in nonprimary vibration direction on the (here, it is x-axis as a representative) without compensation for cross-axis sensitivity, ΔS_{C_YN} and ΔS_{C_ZN} refer to the wavelength change rate of the sensor owing to the cross-axis sensitivities corresponding to the nonprimary y- and z-directions of motion, respectively, $\Delta\lambda_Y$ and $\Delta\lambda_Z$ refer to the wavelength change corresponding to the nonprimary direction, and $\Delta\lambda_{X+Y+Z}$ is the summation of the wavelength change in three axis directions. The use of the ± symbol in (11) indicates that if the wavelength shift is positive, it should be reduced by the cross-axis sensitivity, whereas if the wavelength shift is negative, it should be increased by the cross-axis sensitivity.

Using the expression given by (11), when the acceleration is applied along the x-axis, the wavelength shifts in the y- and z-axis directions can be decreased by the cross-axis sensitivity. Fig. 5 shows the results of compensating for the cross-axis sensitivity, indicating that the sensitivity and linearity of the target acceleration sensor were not significantly affected by the compensation for cross-axis sensitivity, but the cross-axis sensitivity itself was significantly reduced from 4.7% to 1.8%.

D. Evaluation As an IMU

A linear acceleration sensor can measure the change in linear acceleration, but also enables the measurement of gravity. An

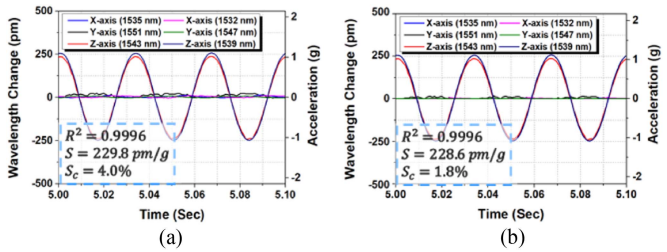

Fig. 5. Wavelength shifts over time (a) before and (b) after compensating for cross-axis sensitivity.

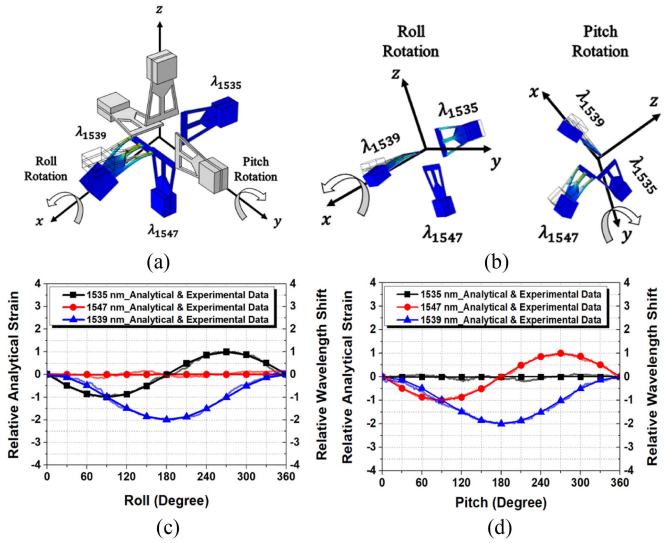

Fig. 6. (a) Definition of roll & pitch angle and corresponding cantilever (blue color). (b) Change in cantilevers during rotation. (c) Analytically and experimentally determined variation in wavelength shift according to change in roll and (d) pitch angles.

appropriate arrangement of three or more acceleration sensors can therefore be used to measure changes in gravitational acceleration according to changes in the roll and pitch angles of the target object. Under slow rotational speeds, it is more efficient to measure the rotation angle through the change in the value of gravitational acceleration than to directly obtain a roll and pitch angle through the change in angular acceleration. The change in roll and pitch angle can then be obtained using a simple relational equation. In this study, a Madgwick filter was slightly modified and used to calculate the accuracy of the roll and pitch angles measured by the FBG linear/angular acceleration sensor [25].

Fig. 6(a) and (b) define the directions of roll and pitch considered in this study based on the initial state of the FBG linear/angular acceleration sensor as well as the three cantilevers (1535, 1539, and 1547 nm) used to measure the change in roll and pitch angle. The graphs in Fig. 6(c) and (d) show the analytically and experimentally determined changes in the strain and wavelength of the cantilevers according to the changes in the roll and pitch angles. When the roll and pitch angles were rotated by 360°, the absolute wavelength changes occurring in the three cantilevers were converted to relative wavelength changes using the sensor sensitivity and inserted into the modified Madgwick filter. This process converted the relative wavelength change

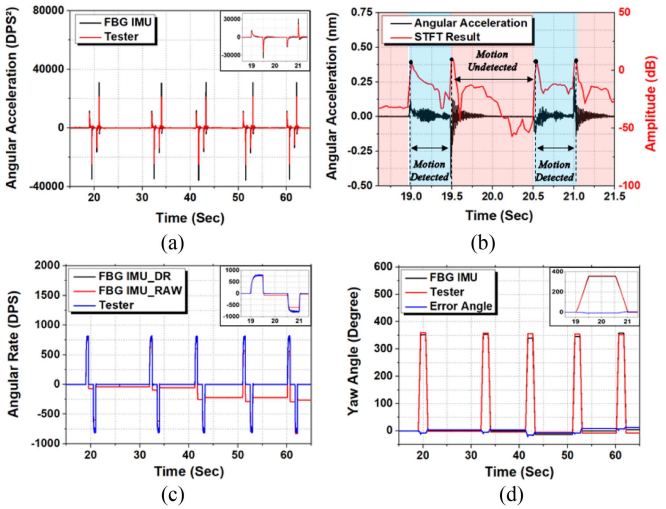

Fig. 7. Yaw angle measurement performance evaluation. (a) Wavelength shift data before/after notch filters application. (b) Drift rates generated during angular acceleration measurement. (c) Angular velocity obtained through primary integration. (d) Yaw angles obtained through secondary integration.

values into x-, y-, and z -acceleration values used to calculate the roll and pitch angles.

An finite elements method (FEM) simulation was conducted to obtain the relative strain value when the three cantilevers were rotated 360° in the roll and pitch directions under the same conditions as the experiment; the simulation results were quite similar to the experimental results. The analytically obtained relative strain values could also be calculated as the analytical values of roll and pitch when given as inputs to the modified Madgwick filter. This approach indicated that the average roll and pitch error angles of the FBG linear/angular acceleration sensor were 3.98 and 4.72°, respectively, throughout a 360° rotation.

The roll and pitch angles were also tracked using the changes in gravitational acceleration (linear acceleration) without the help of angular acceleration measurements; an approach adopted by several current commercial acceleration sensors [25]. One of the critical differences between commercial acceleration sensors and the proposed FBG linear/angular acceleration sensor is that the latter can directly measure the angular acceleration and estimate the yaw angle accordingly. To evaluate the ability of the proposed sensor to obtain the change in the rotational yaw angle using the measured angular acceleration data, an experiment was conducted to estimate the change in yaw angle through double integration.

Fig. 7 shows the results of rotating the FBG linear/angular acceleration sensor connected to the encoder motor by 360° in the CW direction and then 360° in the CCW direction for a total of 720° of rotation; this rotational scheme was applied five times. Notably, tracking the yaw angle requires a signal processing algorithm that operates differently from the roll and pitch angle calculations. Thus, the bias for the entire raw dataset was first corrected, and the vibration component

TABLE I
PERFORMANCE OF FBG LINEAR/ANGULAR ACCELERATION SENSOR

Sensor Type	Parameter	Value
Linear Acceleration	Full-Scale Range	±14 g
	Average Scale Factor	201.4–259.5 pm/g
	Nonlinearity	±0.05%
	RMS Noise	10.04 mg
	Cross-axis Sensitivity	±1.8% (Compensated)
Angular Acceleration	Average Scale Factor	20~22 °/s²/pm
	Nonlinearity	±0.23%
	Cross-axis Sensitivity	< 1.6%
Inertial Measurement	Roll Angle Accuracy	1.11% (3.98°)
	Pitch Angle Accuracy	1.31% (4.72°)
	Yaw Angle Accuracy	0.54% (3.89°)

of the cantilever was removed using a notch filter. The peak frequency, which is the main parameter of the notch filter, was set to 46 Hz considering the resonant frequency of 46.366 Hz obtained through an FEM analysis of the resonant frequency of the cantilever. The measurement noise component of the data that passed through the notch filter was removed using the low-pass filter, and the amplitude lost owing to filtering was restored. Applying an angular acceleration sensor sensitivity of ~20 to 22°/s²/pm, (More information on the sensitivity of angular acceleration were shown in Fig. S3 of the Supplementary material), the measured wavelengths were converted into the angular acceleration values shown in Fig. 7(a). Next, a general dead-reckoning method was used to obtain the angular velocity at which the drift components were removed. To determine the drift-reduced angular velocity, the zero-velocity update method and linear drift model were adopted [26]. The moving and nonmoving sections were separated using the short-time Fourier transform, which is frequently used to distinguish movements in gait analysis, as shown in Fig. 7(b). The drifts occurring at the start and end points of the movement were considered to be either linear increases or decreases and compensated for accordingly. The angular velocity data obtained through drift compensation was then confirmed against the values reported by the tester in the blue graph shown in Fig. 7(c). Finally, the data were integrated once more, and the change in the yaw angle was estimated as shown in Fig. 7(d).

Notably, the signal processing discussed in this section can be conducted using postprocessing techniques rather than real-time processing, And the detailed filtering process is in Fig. S4 of the Supplementary material. However, the yaw angle obtained through this process exhibited an error when compared with the yaw angle obtained through the encoder motor. The average error angle that occurred during five 720° rotations was ~3.89°, which equated to an error rate of 0.54%.

E. Discussion

As can be seen in Table I, the measurement range of the FBG acceleration sensor evaluated through simulation was ±14 g. Considering that a typical MEMS IMU sensor used for motion capture has a maximum measurement range of ±16 g

and the maximum instantaneous linear acceleration occurring in human movement is less than 10 g, the proposed FBG linear/angular acceleration sensor has sufficient capabilities to satisfy the motion capture industry [27]. In addition, the average sensor sensitivity of 229.4 pm/g is more than twice that of the one-axis FBG acceleration sensor deployed in commercial industry, which is about 100 pm/g [28]. The nonlinearity of the linear acceleration sensor was within $\pm 0.05\%$, which is in the range ($<0.1\%$) provided by the gyroscope sensor in a tactical grade IMU sensor; the nonlinearity of the angular acceleration sensor was only $\pm 0.23\%$, showing excellent characteristics. It was confirmed that the cross-axis sensitivity of the proposed linear/angular acceleration sensor was within 2.0% (The cross-axis sensitivity of angular acceleration measurements was discussed in Fig. S5 of the Supplementary material.) after compensation, which matches the sensitivity of a commercial automotive grade MEMS IMU sensor. The roll and pitch angles determined using the gravitational acceleration measured by the linear acceleration sensor showed an average error of 3.98 to 4.72° when rotating 360°, representing an accuracy of $\sim$1.11 to 1.31%. The yaw angle measured by the angular acceleration sensor indicated an average error angle of 3.89° or an accuracy of 0.54% when a 720° rotation was performed five times.

IV. Conclusion

To overcome the shortcomings of conventional MEMS-based IMU sensors, a novel sensor comprising six cantilever-type accelerometers each incorporating an FBG sensor that is unaffected by EMI was proposed in this study to measure the linear/angular acceleration of an object through the deformation of the FBG sensors. The results of the experiments and simulations conducted in this study indicated that the proposed sensor can be used to track the movement of an object within the tolerances for traditional IMU sensors without the risk of interference.

The proposed FBG linear/angular acceleration sensor can be used for earthquake prediction and angular vibration analysis of structures, but it was primarily developed to serve as an IMU sensor capable of estimating roll, pitch, and yaw angles through measurements of gravity and double integrations of measured angular acceleration. The results presented in this article can therefore be actively used as a basis for the development of high-precision IMU sensors for use in future industrial applications subjected to environmental noise such as EMI.

References

[1] S. Jung, Y. Cho, K. Lee, and M. Chang, "Moving object detection with single moving camera and IMU sensor using mask R-CNN instance image segmentation," *Int. J. Precis. Eng. Manuf.*, vol. 22, no. 6, pp. 1049–1059, 2021.

[2] B. Li, C. Zhang, C. Ye, W. Lin, X. Yu, and L. A. Meng, "Robust odometry algorithm for intelligent railway vehicles based on data fusion of encoder and IMU," in *Proc. IEEE Ind. Electron. Soc.*, pp. 2749–2753, 2020.

[3] J. Henawy, Z. Li, W. Y. Yau, and G. Seet, "Accurate IMU factor using switched linear systems for VIO," *IEEE Trans. Ind. Electron.*, vol. 68, no. 8, pp. 7199–7208, Aug. 2021.

[4] C. M. Lee, J. Park, S. Park, and C. H. Kim, "Fall-detection algorithm using plantar pressure and acceleration data," *Int. J. Precis. Eng. Manuf.*, vol. 21, no. 4, pp. 725–737, 2020.

[5] Q. Zhang, Y. Hu, S. Li, T. Zhang, and X. Niu, "Mounting parameter estimation from velocity vector observations for land vehicle navigation," *IEEE Trans. Ind. Electron.*, vol. 69, no. 4, pp. 4234–4244, Apr. 2022.

[6] D. Rojas-Rueda, M. J. Nieuwenhuijsen, H. Khreis, and H. Frumkin, "Autonomous vehicles and public health," *Annu. Rev. Public Health*, vol. 41, no. 1, pp. 329–345, 2020.

[7] A. R. Ruddle, "Preliminary estimates of electromagnetic field exposures due to advanced vehicle technologies," in *Proc. Loughborough Antennas Propag. Conf.*, 2016, pp. 1–5.

[8] W. Gao, H. Wang, D. Fang, Y. Wang, H. Zhang, and X. Zhang, "Auxiliary error correction method for high precision IMU," *Proc. IOP Conf. Ser., Mater. Sci. Eng.*, vol. 612, no. 4, Oct. 2019, Art. no. 042063.

[9] M. Zhang, M. Zhang, Y. Chen, and M. Li, "IMU data processing for inertial aided navigation: A recurrent neural network based approach," in *Proc. IEEE Int. Conf. Robot. Automat.*, 2021, pp. 3992–3998.

[10] J. Y. Kim, J. Y. Kim, H. S. Kim, and K. Park, "Development and evaluation of a hybrid walking rehabilitation robot DDgo pro," *Int. J. Precis. Eng. Manuf.*, vol. 21, no. 11, pp. 2105–2115, 2020.

[11] G. Ariante, U. Papa, S. Ponte, and G. Del Core, "UAS for positioning and field mapping using LIDAR and IMU sensors data: Kalman filtering and integration," in *Proc. IEEE 5th Int. Workshop Metrol. Aerosp.*, Jun. 2019, pp. 522–527.

[12] D. Fedasyuk, R. Holyaka, and T. Marusenkova, "A tester of the MEMS accelerometers operation modes," in *Proc. Int. Conf. Adv. Inf. Commun. Technol.*, 2019, pp. 227–230.

[13] J. Mendoza-Choquemamani, B. Espinoza-Garcia, J. C. Cutipa-Luque, and P. R. Yanyachi, "Comparison and evaluation between a low-cost IMU and INS VN-300 in AHRS mode," in *Proc. IEEE Int. Conf. Aerosp. Signal Process.*, 2021, pp. 1–4.

[14] M. Ilyas, K. Cho, S. H. Baeg, and S. Park, "Drift reduction in pedestrian navigation system by exploiting motion constraints and magnetic field," *Sensor*, vol. 16, no. 9, 2016, Art. no. 1455.

[15] Y. Chen, W. Hu, Y. Yang, J. Hou, and Z. Wang, "A method to calibrate installation orientation errors of inertial sensors for gait analysis," in *Proc. IEEE Int. Conf. Inf. Autom.*, 2014, pp. 598–603.

[16] Q. Zhou, G. Yu, H. Li, and N. Zhang, "A novel MEMS gyroscope in self-calibration approach," *Sensor*, vol. 20, no. 18, 2020, Art. no. 5430.

[17] T. Zou, F. Ni, C. Guo, K. Li, and H. Liu, "A 6-DOF acceleration sensor with cylindrical configuration," *Sens. Actuators A, Phys.*, vol. 251, pp. 167–178, 2016.

[18] P. Cardou, G. Fournier, and P. Gagnon, "A nonlinear program for angular-velocity estimation from centripetal-acceleration measurements," *IEEE/ASME Trans. Mechatronics*, vol. 16, no. 5, pp. 932–944, Oct. 2011.

[19] H. C. Lefèvre, "The fiber-optic gyroscope: Challenges to become the ultimate rotation-sensing technology," *Opt. Fiber Technol.*, vol. 19, no. 6, pp. 828–832, 2013.

[20] M. J. Caruso, "Applications of magnetic sensors for low cost compass systems," in *Proc. IEEE Position Location Navig. Symp.*, 2000, pp. 177–184.

[21] L. Xiong, Y. Guo, G. Jiang, X. Zhou, L. Jiang, and H. Liu, "Six-dimensional force/torque sensor based on fiber Bragg gratings with low coupling," *IEEE Trans. Ind. Electron.*, vol. 68, no. 5, pp. 4079–4089, May 2021.

[22] L. Jin et al., "Two-dimensional bend sensing with a cantilever-mounted FBG," *Meas. Sci. Technol.*, vol. 17, no. 1, 2005, Art. no. 168.

[23] L. Xiang, Q. Jiang, Y. Li, and R. Song, "Design and experimental research on cantilever accelerometer based on fiber Bragg grating," *Opt. Eng.*, vol. 55, no. 6, 2016, Art. no. 066113.

[24] T. Hiller, L. Blocher, M. Vujadinović, Z. Péntek, A. Buhmann, and H. Roth, "Analysis and compensation of cross-axis sensitivity in low-cost MEMS inertial sensors," in *Proc. IEEE Int. Symp. Inertial Sens. Syst.*, 2021, pp. 1–4.

[25] S. Madgwick, "An efficient orientation filter for inertial and inertial/magnetic sensor arrays," *Rep. x-io Univ. Bristol (U.K.)*, vol. 25, pp. 113–118, 2010.

[26] F. Dadashi, G. Millet, and K. Aminian, "Approaching on-line estimation of swimming instantaneous velocity using a wearable IMU," in *Proc. Int. Symp. 3D Anal. Hum. Movement*, 2014, pp. 176–179.

[27] D. A. Bruening, R. E. Reynolds, C. W. Adair, P. Zapalo, and S. T. Ridge, "A sport-specific wearable jump monitor for figure skating," *PLoS One*, vol. 13, no. 11, 2018, Art. no. e0206162.

[28] P. F. C. Antunes, C. A. Marques, H. Varum, and P. S. Andre, "Biaxial optical accelerometer and high-angle inclinometer with temperature and cross-axis insensitivity," *IEEE Sens. J.*, vol. 12, no. 7, pp. 2399–2406, Jul. 2012.

Byung Kook Kim received the M.S. degree in the development of a human body motion capture system using an FBG optical fiber sensor, a wearable hand motion capture module using an FBG angle sensor, and a combination FBG sensor hardware/software systems from the Mechanical Engineering Department, Yonsei University, Seoul, South Korea, in 2017. He is currently working toward the Ph.D. degree with the Korea Institute of Science and Technology, Seoul, associated with Yonsei University.

His research interests include the development of a human body motion capture system using an FBG optical fiber sensor, a wearable hand motion capture module using an FBG angle sensor, and a combination FBG sensor hardware/software systems. For the present study, he provided the concept for FBG linear/angular acceleration sensors, the design of experimental analysis and signal processing algorithms, and experimental/theoretical/numerical analyses/comparisons using FEM simulations.

Minsu Jang received the Ph.D. degree in the development of a human body motion capture system using FBG optical fiber sensors, measurement of shape changes in three-dimensional space using FBG sensors, and production of FBG shape sensors for fingers and colonoscopy equipment from the School of Chemical Engineering, Sungkyunkwan University, Seoul, South Korea, in 2019.

He is currently a Postdoctoral Researcher with the Korea Institute of Science and Technology, Seoul. His research interests include the development of a human body motion capture system using FBG optical fiber sensors, measurement of shape changes in three-dimensional space using FBG sensors, and production of FBG shape sensors for fingers and colonoscopy equipment. For the present study, he proposed the approach for the improvement of FBG linear/angular acceleration sensor, specific directions for sensor experiments using FBG optical fibers, and comprehensive guidance for FBG sensors and interrogator systems.

Jun Sik Kim received the M.S. degree in the production of FBG angle sensors and their application to hand motion capture, and the use of ultra-small MEMS-based FBG sensors in motion capture industries from the School of Electrical Engineering, Korea University, Seoul, South Korea, in 2020.

He is currently an employee of the C&C Process Technical Department, KCTech, Icheon, South Korea. His research interests include the production of FBG angle sensors and their application to hand motion capture, and the use of ultra-small MEMS-based FBG sensors in motion capture industries. For the present study, he presented experimental advice for designing the FBG sensor manufacturing process.

Kyumin Kang received the M.S. degree in the development of an interrogator signal processing algorithm through optical spectral analysis and the design of a multichannel/high-power FBG integrator from the School of Electrical Engineering, Korea University, Seoul, South Korea, in 2021. He is currently working toward the Ph.D. degree in the Department of Electrical and Computer Engineering, Sungkyunkwan University, Seoul.

His research interests include the development of an interrogator signal processing algorithm through optical spectral analysis and the design of a multichannel/high-power FBG integrator. For the present study, he provided comprehensive advice for analyzing the FBG linear/angular acceleration wavelength.

Dae-Eun Kim received the Ph.D. degree in the tribology of materials, including most research topics related to contact systems and he deals with in-depth research topics such as durability tests to secure mechanical properties, hardware system design, and FEM simulation verification of hardware systems from the Department of Mechanical Engineering, Massachusetts Institute of Technology, Cambridge, MA, USA, in 1991.

He is currently a Professor with the Tribology Research Lab, Yonsei University, Seoul, South Korea. His research interests include the tribology of materials, including most research topics related to contact systems and he deals with in-depth research topics such as durability tests to secure mechanical properties, hardware system design, and FEM simulation verification of hardware systems. For the present study, he presented scientific and theoretical guidance in areas such as the manufacturing process of FBG acceleration sensors, FEM simulation verification process, and analysis of the mechanical characteristics of sensor systems.

Jinseok Kim received the Ph.D. degree in electrical engineering and computer science from Seoul National University, Seoul, South Korea, in 2007.

He is currently a Senior Researcher with the Center for Bionics, Korea Institute of Science and Technology, Seoul. His research interests include the development of FBG sensors (curvature sensors, shape sensors, and torsion sensors) for motion capture, development of fiber-based wearable suits for motion capture and rehabilitation industries, and sensor targeting designs for specific applications. For the present study, he provided guidance on the design and direction of experimental equipment for FBG linear/angular acceleration sensors and theoretical/comprehensive guidance on the signal processing of acceleration measurements.